
Sampling in Unit Time with Kernel Fisher–Rao Flow

Aimee Maurais & Youssef Marzouk
 Center for Computational Science and Engineering
 Massachusetts Institute of Technology
 Cambridge, MA 02139
 {maurais, ymarz}@mit.edu

Abstract

We introduce a new mean-field ODE and corresponding interacting particle systems for sampling from an unnormalized target density or Bayesian posterior. The interacting particle systems are gradient-free, available in closed form, and only require the ability to sample from the reference density and compute the (unnormalized) target-to-reference density ratio. The mean-field ODE is obtained by solving a Poisson equation for a velocity field that transports samples along the geometric mixture of the two densities $\pi_0^{1-t}\pi_1^t$, which is the path of a particular Fisher–Rao gradient flow. We employ a reproducing kernel Hilbert space ansatz for the velocity field, which makes the Poisson equation tractable and enables us to discretize the resulting mean-field ODE over finite samples, as a simple interacting particle system. The mean-field ODE can be additionally be derived from a discrete-time perspective as the limit of successive linearizations of the Monge–Ampère equations within a framework known as sample-driven optimal transport. We demonstrate empirically that our interacting particle systems can produce high-quality samples from distributions with varying characteristics.

1 Introduction

In this work we consider the problem of *sampling via transport*: given a target distribution π_1 on \mathbb{R}^d and a reference π_0 on \mathbb{R}^d from which we can sample, our goal is to find $T : \mathbb{R}^d \rightarrow \mathbb{R}^d$ such that $T_{\#}\pi_0 = \pi_1$, i.e., $X_0 \sim \pi_0 \Rightarrow T(X_0) \sim \pi_1$. We assume that π_0 and π_1 both admit densities and that we can evaluate the (unnormalized) *density ratio*¹ $\frac{\pi_1}{\pi_0}$ but do not have samples of π_1 with which to train the map or access to gradients, including scores, of π_1 or π_0 . The target-to-reference density ratio is available when the density of π_1 is known and π_0 is chosen to be some “standard” reference (e.g., Gaussian), but is also accessible in the Bayesian setting so long as the likelihood function is known: therein $\pi_1 \propto \ell \pi_0$ for some likelihood $\ell(x) = \pi(y^*|x)$, and hence the ratio is $\frac{\pi_1}{\pi_0} \propto \ell$. We thus use the term “likelihood” to refer to the ratio $\frac{\pi_1}{\pi_0}$ throughout this paper.

The canonical sampling approach employing the likelihood is importance sampling [39], which transforms an unweighted ensemble of samples of π_0 into a *weighted* ensemble, enabling the estimation of expectations under π_1 . Importance sampling is the foundation for sequential Monte Carlo (SMC) methods [15], but is frequently plagued by issues of weight degeneracy and ensemble collapse, necessitating large ensemble sizes [46] or interventions such as resampling [32] and MCMC rejuvenation.

Importance weights can alternately be used as *ingredients* to build transport maps which, when applied to samples from π_0 , yield *uniformly* weighted approximate samples from π_1 . This strategy is

¹For the remainder of this paper, the terms “density” and “density ratio” refer to unnormalized quantities unless otherwise stated.

employed in the analysis step of the ensemble transform particle filter of [43], wherein importance weights are used to define the marginals of a discrete optimal transport (OT) problem and the resulting OT coupling used as a Bayesian prior-to-posterior transformation. While this approach is shown to be consistent and has the benefit of being nonparametric, the transformation obtained is linear and transformed samples cannot leave the convex hull of the originals. However, the basic premise of [43]—using importance weights to define optimal transport problems—is nonetheless an inspiration for an approach we use here to find incremental OT maps within a homotopy method for transport.

Many sampling approaches use *dynamics* to define a transport, e.g., via the flow map induced by trajectories of an ODE or the stochastic mapping induced by sample paths of an SDE. In either case, the idea is to apply dynamics which will transform some initial state $X_0 \sim \pi_0$ to a state $X_S \sim \pi_{X_S} \approx \pi_1$ for some time $S > 0$. This approach underlies flow, diffusion, and bridge techniques for generative modeling, e.g., [14, 31, 34, 36, 58, 1, 47], wherein samples from both π_0 and π_1 are almost always required for training (with [56, 26] being recent exceptions). In the setting where π_1 is known only through its unnormalized density, there are a number of dynamic sampling algorithms which have their grounding as *gradient flows* of functionals on spaces of probability measures. There are several geometries in which one may define gradient flows on probability measures (see [9] for a helpful review), but most well-known algorithms in this vein (e.g., [35, 21, 22, 44]) use some form of the Wasserstein geometry [57] to define dynamics which must, in principle, be run for *infinite time* in order to ensure correct sampling from π_1 .

In this work we develop a dynamic sampling approach based on an ODE which transports samples from π_0 to π_1 in *unit time* such that the time-dependent distribution of the samples is the geometric mixture $\pi_t \propto \pi_0^{1-t} \pi_1^t = \pi_0 \left(\frac{\pi_1}{\pi_0}\right)^t$, $t \in [0, 1]$. Although our algorithms are gradient-free and only require the likelihood $\frac{\pi_1}{\pi_0}$, the path of distributions π_t corresponds to the Fisher–Rao gradient flow of the expected negative log likelihood. The underlying dynamics are described by a **mean-field ODE model**, which we show is the limit of two different **interacting particle systems**. These interacting particle systems, which we generally refer to as *Kernel Fisher–Rao Flow*, are obtained in two distinct but related ways. On one hand, in continuous time, the mean-field ODE can be obtained from the weak formulation of a Poisson equation for a *velocity field* defined in a reproducing kernel Hilbert space (RKHS), from which we obtain a finite-particle ODE system by approximating expectations via Monte Carlo. On the other, in discrete time, one can approximate the optimal transport *map* which pushes π_t to $\pi_{t+\Delta t}$ via linearization of the Monge–Ampère equations discretized over finitely many kernel basis functions and finitely many samples. This linearization yields an interacting particle system which in discrete time is distinct from, but in continuous time identical to, that obtained via the RKHS approach to Poisson’s equation.

The paper is organized as follows: in Section 2, we review existing approaches to sampling via transport with particular emphasis on homotopy approaches which employ the geometric mixture. In Section 3, we derive the mean-field ODE model via solution of Poisson’s equation in an RKHS and introduce an interacting particle system which attains this mean-field ODE as its continuum limit. In Section 4 we derive the mean-field ODE from an alternative, discrete-time perspective as the continuous-time limit of incremental transport maps computed with sample-driven optimal transport. Numerical examples are given in Section 5, and closing remarks in Section 6.

2 Background

Sampling via measure transport is an active area of research, with many computational approaches [37, 29, 40, 55] appearing in recent years. Most practical transport maps are parameterized, and thus a crucial part of realizing them is selecting an appropriately rich function class within which to search for the map. Common map approximation classes include polynomials [41, 3], radial basis functions [49], composed simple transformations [45, 40, 29], neural networks [7, 52, 2], and reproducing kernel Hilbert spaces [35, 31, 28]. Determining an appropriate basis to represent a transport map can be challenging, especially when the target and reference distributions are high-dimensional or differ from each other considerably. For this reason it may be necessary to employ, e.g., adaptive feature selection algorithms [3] or dimension reduction techniques [48, 8, 6, 11].

As an alternative to searching for a single, potentially highly complex transport map which pushes the reference π_0 directly to the target π_1 , one can instead prescribe a *path* of distributions $(\pi_t)_{t \in [0,1]}$ having the target and reference as endpoints and seek a sequence of maps T_1, \dots, T_N which push

samples along a discretization of the path, as depicted in Figure 1. The composed map $T = T_N \circ T_{N-1} \circ \dots \circ T_1$ pushes forward π_0 to π_1 . In continuous time this approach becomes one of finding a *velocity field* $v_t : \mathbb{R}^d \rightarrow \mathbb{R}^d$ such that the solution to the initial value problem

$$\dot{X}_t = v_t(X_t), \quad X_0 \sim \pi_0$$

has distribution π_t . Samplers of unnormalized densities which employ this homotopy approach frequently take π_t to be the geometric mixture

$$\pi_t \propto \pi_0^{1-t} \pi_1^t = \pi_0 \left(\frac{\pi_1}{\pi_0} \right)^t, \quad t \in [0, 1], \quad (1)$$

which interpolates between π_0 and π_1 in unit time. This mixture may be referred to as the “power posterior” path and appears, for example, in annealed importance sampling [38, 4, 30, 25] and parallel tempering [23, 19, 51]. In Bayesian computation, this path is sometimes referred to as “tempered likelihood” and has been used as the basis for algorithms which generate (approximate) posterior samples [42, 13, 27, 17] or posterior densities [16].

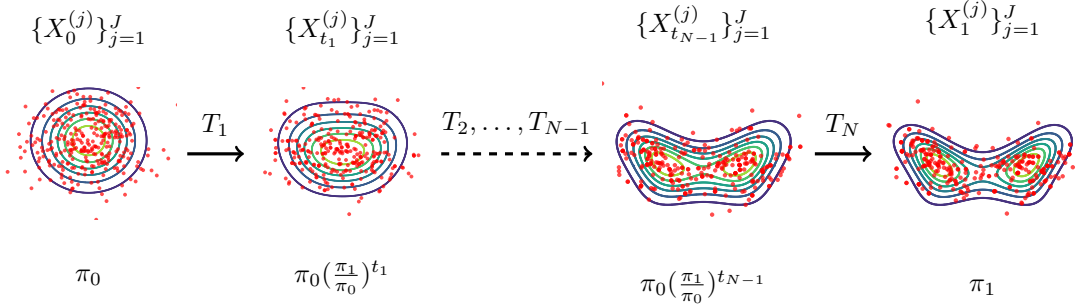


Figure 1: We employ a homotopy-based sampling scheme in this work, deriving a mean-field ODE which approximately transports a reference π_0 to a target π_1 in unit time. In discrete time this approach amounts to obtaining incremental transport maps T_1, \dots, T_N .

The idea of using the tempered likelihood path to sample the posterior distribution in Bayesian inference was, to our knowledge, first developed in [12, 42] in the context of filtering. In [12, 13] and related works by the same authors, the tempered likelihood is used to derive ODEs and SDEs for nonlinear filtering in full generality, and as such these systems require gradients and even Hessians of the likelihood and prior. The algorithms for propagating samples from prior to posterior along the tempered likelihood in [42] are simpler, but are of ensemble-Kalman type and employ a Gaussian approximation for each π_t , meaning that their expressivity is limited. A similar methodology to [42], now known as Ensemble Kalman Inversion (EKI), was proposed for computing point estimates in the context of Bayesian inverse problems in [27]. The iteration underlying EKI is run for infinite time, but, as noted in, e.g., [17], when the iteration is stopped at $t = 1$ samples from a Gaussian approximation to the posterior are obtained. Even in the limit of infinite particles and continuous time, however, ensemble Kalman methods are not consistent samplers for general (i.e., non-Gaussian) posteriors [17].

The mean-field ODE model and interacting particle systems we introduce here can be seen as extensions of the tempered likelihood methodology [42, 13] to the more general problem of sampling from unnormalized probability measures. We introduce RKHS techniques for approximating the solution to the Poisson equation defining the velocity field, which (i) enable greater expressivity than ensemble Kalman techniques based on Gaussian approximations and (ii) yield a mean-field ODE which gives rise to simple, closed-form, deterministic, and gradient-free interacting particle systems.

Notation We use $K(\cdot, \cdot) : \mathbb{R}^d \times \mathbb{R}^d \rightarrow \mathbb{R}$ to represent a symmetric positive definite kernel on \mathbb{R}^d and denote by $(\mathcal{H}_K, \langle \cdot, \cdot \rangle_{\mathcal{H}_K})$ the reproducing kernel Hilbert space [50] associated with K . We assume that $K(\cdot, x)$ is C^2 and use $\nabla_1 K(\cdot, \cdot)$ to refer to the gradient of K with respect to the first argument and $\nabla_2 K(\cdot, \cdot)$ to refer to the gradient with respect to the second. $\mathcal{P}_{2,ac}(\mathbb{R}^d)$ denotes the space of probability measures on \mathbb{R}^d with finite second moments and which admit densities.

3 Methodology: Poisson's equation in reproducing kernel Hilbert space

Our goal is to find a time-varying velocity field $v_t : \mathbb{R}^d \rightarrow \mathbb{R}^d$ such that the distribution of X_t evolving according to

$$\dot{X}_t = v_t(X_t), \quad X_0 \sim \pi_0 \quad (2)$$

is the geometric mixture (1). Had we access to such a velocity field, we could obtain samples from π_1 by sampling π_0 and simulating the dynamics (2) for unit time. It can be shown that π_t in (1) satisfies

$$\partial_t \pi_t = \pi_t \left(\log \frac{\pi_1}{\pi_0} - \mathbb{E}_{\pi_t} \left[\log \frac{\pi_1}{\pi_0} \right] \right),$$

which is the Fisher–Rao gradient flow of the functional $\mathcal{F} : \mathcal{P}_{2,ac}(\mathbb{R}^d) \rightarrow \mathbb{R}$ defined

$$\mathcal{F}(\pi) = -\mathbb{E}_{\pi} \left[\log \frac{\pi_1}{\pi_0} \right].$$

$\mathcal{F}(\pi)$ is the expected negative log likelihood under π . Using the continuity equation, a velocity field in (2) yielding $X_t \sim \pi_t$ must then satisfy

$$-\nabla \cdot (\pi_t v_t) = \pi_t \left(\log \frac{\pi_1}{\pi_0} - \mathbb{E}_{\pi_t} \left[\log \frac{\pi_1}{\pi_0} \right] \right). \quad (3)$$

There are many possible solutions to the PDE (3), but if, as in [53, 42], we insist that in the limit $\Delta t \rightarrow 0$ the expected transportation cost $\frac{1}{\Delta t^2} \mathbb{E}_{\pi_t} [\|X_t - X_{t+\Delta t}\|^2]$ is minimized for each t , we obtain a constrained optimization problem for each v_t with a unique solution,

$$\min_{v_t : \mathbb{R}^d \rightarrow \mathbb{R}^d} \int_{\mathbb{R}^d} \|v_t\|^2 d\pi_t \quad \text{s.t.} \quad -\nabla \cdot (\pi_t v_t) = \pi_t \left(\log \frac{\pi_1}{\pi_0} - \mathbb{E}_{\pi_t} \left[\log \frac{\pi_1}{\pi_0} \right] \right).$$

It can be shown by calculus of variations [42] that the optimal solution to this problem is $v_t = \nabla u_t$, where u_t satisfies the Poisson equation

$$-\nabla \cdot (\pi_t \nabla u_t) = \pi_t \left(\log \frac{\pi_1}{\pi_0} - \mathbb{E}_{\pi_t} \left[\log \frac{\pi_1}{\pi_0} \right] \right). \quad (4)$$

We make (4) tractable by searching for u_t in the RKHS \mathcal{H}_K , i.e., taking $u_t(\cdot) = \int_{\mathbb{R}^d} K(\cdot, x) f_t(x) d\pi_t(x)$ for some $f_t : \mathbb{R}^d \rightarrow \mathbb{R}$, and enforcing the weak form of (4), as in [33], for kernel test functions $K(\cdot, x)$,

$$\int_{\mathbb{R}^d} \langle \nabla_1 K(y, x), \nabla u_t(y) \rangle d\pi_t(y) = \int_{\mathbb{R}^d} K(y, x) \left(\log \frac{\pi_1}{\pi_0}(y) - \mathbb{E}_{\pi_t} \left[\log \frac{\pi_1}{\pi_0} \right] \right) d\pi_t(y) \quad \forall x \in \mathbb{R}^d. \quad (5)$$

Substituting the form of u_t into (5), we have for all $x \in \mathbb{R}^d$

$$\begin{aligned} M_{\pi_t} f_t(x) &\equiv \iint_{\mathbb{R}^d \times \mathbb{R}^d} f_t(z) \langle \nabla_1 K(y, x), \nabla_1 K(y, z) \rangle d\pi_t(y) d\pi_t(z) \\ &= \int_{\mathbb{R}^d} K(x, y) \left(\log \frac{\pi_1}{\pi_0}(y) - \mathbb{E}_{\pi_t} \left[\log \frac{\pi_1}{\pi_0} \right] \right) d\pi_t(y) \equiv K_{\pi_t} \left(\log \frac{\pi_1}{\pi_0} - \mathbb{E}_{\pi_t} \left[\log \frac{\pi_1}{\pi_0} \right] \right) (x), \end{aligned}$$

where, for functions $g : \mathbb{R}^d \rightarrow \mathbb{R}$, M_{π_t} is the integral operator

$$\begin{aligned} M_{\pi_t} g(\cdot) &= \int_{\mathbb{R}^d} g(z) \mathbb{E}_{X_t \sim \pi_t} [\langle \nabla_1 K(X_t, \cdot), \nabla_1 K(X_t, z) \rangle] d\pi_t(z) \\ &= \iint_{\mathbb{R}^d \times \mathbb{R}^d} g(z) \langle \nabla_1 K(y, x), \nabla_1 K(y, z) \rangle d\pi_t(y) d\pi_t(z) \end{aligned}$$

and K_{π_t} is the kernel integral operator $K_{\pi_t} g(\cdot) = \int_{\mathbb{R}^d} g(z) K(\cdot, z) d\pi_t(z)$. Under the condition that M_{π_t} is invertible, then, f_t is given by $f_t(\cdot) = M_{\pi_t}^{-1} K_{\pi_t} \left(\log \frac{\pi_1}{\pi_0} - \mathbb{E}_{\pi_t} \left[\log \frac{\pi_1}{\pi_0} \right] \right)$ and we have $v_t = \nabla u_t$ equal to

$$v_t(\cdot) = \int_{\mathbb{R}^d} \nabla_1 K(\cdot, x) M_{\pi_t}^{-1} K_{\pi_t} \left(\log \frac{\pi_1}{\pi_0} - \mathbb{E}_{\pi_t} \left[\log \frac{\pi_1}{\pi_0} \right] \right) (x) d\pi_t(x).$$

Therefore the **mean-field ODE**

$$\dot{X}_t = v_t(X_t) = \mathbb{E}_{X' \sim \rho_t} \left[\nabla_1 K(X_t, X') M_{\rho_t}^{-1} K_{\rho_t} \left(\log \frac{\pi_1}{\pi_0} - \mathbb{E}_{\rho_t} \left[\log \frac{\pi_1}{\pi_0} \right] \right) (X') \right],$$

$$X_0 \sim \pi_0, \quad t \in [0, 1] \quad (6)$$

can be used to evolve samples from π_0 such that $\rho_t = \text{Law}(X_t)$ is approximately $\pi_t \propto \pi_0^{1-t} \pi_1^t$, and hence at $t = 1$ they are approximately distributed as π_1 .

We note that the potential u_t obtained by solving a weak-form Poisson equation over RKHS,

$$u_t = \int_{\mathbb{R}^d} K(\cdot, x) M_{\pi_t}^{-1} K_{\pi_t} \left(\log \frac{\pi_1}{\pi_0} - \mathbb{E}_{\pi_t} \left[\log \frac{\pi_1}{\pi_0} \right] \right) (x) d\pi_t(x)$$

is not necessarily a strong solution to (4). For this reason we differentiate between the target path of distributions $\pi_t \propto \pi_0^{1-t} \pi_1^t$ and $\rho_t = \text{Law}(X_t)$. Understanding the difference between these paths and its dependence on the choice of RKHS \mathcal{H}_K is an important area for future work. Empirically we find the quality of samples generated by running a discretization of (6) to be good; see Section 5.

Because the quantities appearing in v_t can be written as expectations with respect to π_t , the mean-field model (6) can be approximated for finite samples as an **interacting particle system**.

Theorem 1 *Consider the interacting particle system*

$$\dot{X}_t^{(j)} = \left(\nabla_1 K(X_t^{(j)}, X_t^{(1)}) \quad \dots \quad \nabla_1 K(X_t^{(j)}, X_t^{(J)}) \right) M_t^{-1}.$$

$$\frac{1}{J} \sum_{k=1}^J \left(\log \frac{\pi_1}{\pi_0}(X_t^{(k)}) - \frac{1}{J} \sum_{i=1}^J \log \frac{\pi_1}{\pi_0}(X_t^{(i)}) \right) \begin{pmatrix} K(X_t^{(k)}, X_t^{(1)}) \\ \vdots \\ K(X_t^{(k)}, X_t^{(J)}) \end{pmatrix}, \quad j = 1, \dots, J \quad (7)$$

with $t \in [0, 1]$, $\{X_0^{(j)}\}_{j=1}^J \stackrel{\text{i.i.d.}}{\sim} \pi_0$, and $M_t \in \mathbb{R}^{J \times J}$ given by

$$(M_t)_{\ell, m} = \frac{1}{J} \sum_{i=1}^J \langle \nabla_1 K(X_t^{(i)}, X_t^{(\ell)}), \nabla_1 K(X_t^{(i)}, X_t^{(m)}) \rangle, \quad \ell, m = 1, \dots, J.$$

The limit of (7) as $J \rightarrow \infty$ is the mean-field ODE (6).

Proof: See Appendix A.1

We refer to the interacting particle system (7) as **Kernel Fisher–Rao Flow (KFRFlow)** and offer a few observations:

- We only require the abilities to sample π_0 and compute the log density ratio $\log \frac{\pi_1}{\pi_0}$ in order to simulate the ODE (7). In particular contrast to most Langevin-based algorithms [35, 22, 44], we do not require gradients, including scores, of π_0 or π_1 .
- KFRFlow is a simple, closed-form ODE and does not require use of numerical optimization to estimate a score or velocity field, as is frequently the case with comparable finite-time dynamic sampling algorithms [56, 34, 1, 47, 29].
- Similarly to SVGD [35], which can be viewed as a Wasserstein gradient flow with kernelized velocity field, KFRFlow is deterministic and can be viewed as a Fisher–Rao gradient flow with kernelized velocity field.
- M_t is the finite-particle analogue of M_{π_t} . A necessary condition for invertibility of M_t , $J \leq dJ$, is satisfied by construction in the IPS (7). This fact can be seen by noting that $M_t = \frac{1}{J} \sum_{i=1}^J \nabla \mathbf{K}_t(X_t^{(i)}) \nabla \mathbf{K}_t(X_t^{(i)})^\top$, where $\mathbf{K}_t : \mathbb{R}^d \rightarrow \mathbb{R}^J$ is the concatenation $\mathbf{K}_t(\cdot) = (K(\cdot, X_t^{(1)}), \dots, K(\cdot, X_t^{(J)}))^\top$ and $\nabla \mathbf{K}_t \in \mathbb{R}^{J \times d}$ is the Jacobian of \mathbf{K}_t .

Although the mean-field ODE model (6) can perhaps most evocatively be viewed as resulting from the kernelization of a Fisher–Rao gradient flow, it can be recovered separately as the limit of a *discrete-time* interacting particle system obtained using sample-driven optimal transport [31]. We discuss this perspective in the following section.

4 Discrete-time interpretation: sample-driven optimal transport

In discrete time, the problem of finding a velocity field v_t such that the flow $\dot{X}_t = v_t(X_t)$ has distribution $\pi_t \propto \pi_0^{1-t} \pi_1^t$ becomes one of finding transport maps T_1, \dots, T_N which push samples from π_0 along a discretization of π_t . While we can obtain such maps by discretizing the IPS (7), for example taking $X_{t+\Delta t} = X_t + \Delta t \cdot v_t(X_t)$, we can alternately search for the maps *directly* via a framework introduced as sample-driven optimal transport in [54, 31], modified for our setting in which target samples are unavailable.

Suppose that at time $t \in [0, 1)$ we have samples $\{X_t^{(j)}\}_{j=1}^J \sim \pi_t$ which we would like to push forward to $\pi_{t+\Delta t} \propto \pi_t (\frac{\pi_1}{\pi_0})^{\Delta t}$. Given that π_t and $\pi_{t+\Delta t}$ both admit densities, there are many maps $T : \mathbb{R}^d \rightarrow \mathbb{R}^d$ satisfying $T_{\#}\pi_t = \pi_{t+\Delta t}$. The optimal transport approach [57], which we will approximate, is to seek the map which minimizes expected transport cost,

$$\min_{T_{\#}\pi_t = \pi_{t+\Delta t}} \mathbb{E}_{\pi_t} [\|T(X_t) - X_t\|^2]. \quad (8)$$

Owing to the choice of quadratic cost, it can be shown that the optimal map in (8) is the unique convex gradient which pushes forward π_t to $\pi_{t+\Delta t}$ [5]. That is, if we find $T = \nabla\phi$ satisfying $T_{\#}\pi_t = \pi_{t+\Delta t}$ with $\phi : \mathbb{R}^d \rightarrow \mathbb{R}$ convex, we have found the optimal transport map. Thus, we can search for the optimal transport map by seeking $\phi : \mathbb{R}^d \rightarrow \mathbb{R}$ convex such that $\nabla\phi_{\#}\pi_t = \pi_{t+\Delta t}$. The push-forward condition $\nabla\phi_{\#}\pi_t = \pi_{t+\Delta t}$ can be written as a Monge–Ampère PDE [20]

$$\pi_{t+\Delta t}(\nabla\phi(x)) \det(H_\phi(x)) = \pi_t(x),$$

where H_ϕ is the Hessian of ϕ , and interpreted in weak form as

$$\int_{\mathbb{R}^d} f(\nabla\phi(x)) d\pi_t(x) = \int_{\mathbb{R}^d} f(y) d\pi_{t+\Delta t}(y) \quad \forall f : \mathbb{R}^d \rightarrow \mathbb{R} \text{ continuous}. \quad (9)$$

Given that we only have finitely many samples of π_t and access to the ratio $\frac{\pi_1}{\pi_0}$, we arguably do not have enough information to find a map $T = \nabla\phi$ which exactly satisfies $T_{\#}\pi_t = \pi_{t+\Delta t}$. Thus we apply a Galerkin approximation to (9) over a basis of kernel test functions located at each particle, $\{K(\cdot, X_t^{(j)}) : j = 1, \dots, J\}$, seeking a map

$$\nabla\phi_{\mathbf{s}}(x) = x + \sum_{j=1}^J s_j \nabla_1 K(\cdot, X_t^{(j)}), \quad (10)$$

and discretizing the weak form (9) with

$$\int_{\mathbb{R}^d} K(\nabla\phi_{\mathbf{s}}(x), X_t^{(j)}) d\pi_t(x) = \int_{\mathbb{R}^d} K(y, X_t^{(j)}) d\pi_{t+\Delta t}(y), \quad j = 1, \dots, J. \quad (11)$$

Approximating the LHS of (11) via Monte Carlo and the RHS with self-normalized importance sampling, we seek map coefficients $\mathbf{s} = (s_1, \dots, s_m)$ such that

$$\frac{1}{J} \sum_{j=1}^J \mathbf{K}_t(\nabla\phi_{\mathbf{s}}(X_t^{(j)})) = \sum_{j=1}^J w_t^{(j)} \mathbf{K}_t(X_t^{(j)}), \quad w_t^{(j)} = \frac{(\frac{\pi_1}{\pi_0}(X_t^{(j)}))^{\Delta t}}{\sum_{i=1}^J (\frac{\pi_1}{\pi_0}(X_t^{(i)}))^{\Delta t}}, \quad (12)$$

with $\mathbf{K}_t(\cdot) = (K(\cdot, X_t^{(1)}), \dots, K(\cdot, X_t^{(J)}))^{\top}$ as before. Kuang and Tabak [31] refer to the relationship (12) as *sample equivalence* and denote it by $\{\nabla\phi_{\mathbf{s}}(X_t^{(j)})\}_{j=1}^J \sim \{w_t^{(j)} X_t^{(j)}\}_{j=1}^J$. Because we have now discretized the Monge–Ampère equations (9) over finite samples and feature functions, a solution \mathbf{s} to (12) is not guaranteed to yield a unique or optimal map. The *sample-driven* OT problem then, as formulated in [31], is to find a minimum cost map $\nabla\phi_{\mathbf{s}}$ which satisfies sample-equivalence,

$$\min_{\{\nabla\phi_{\mathbf{s}}(X_t^{(j)})\}_{j=1}^J \sim \{w_t^{(j)} X_t^{(j)}\}_{j=1}^J} \sum_{j=1}^J \left\| X_t^{(j)} - \nabla\phi_{\mathbf{s}}(X_t^{(j)}) \right\|^2. \quad (13)$$

Returning to (12), admissible choices of \mathbf{s} in (13) can be identified via root-finding: denote by \mathbf{a} and \mathbf{b} the sample means of \mathbf{K}_t over the unweighted and weighted reference ensembles,

$$\mathbf{a} = \frac{1}{J} \sum_{j=1}^J \mathbf{K}_t(X_t^{(j)}), \quad \mathbf{b} = \sum_{j=1}^J w_t^{(j)} \mathbf{K}_t(X_t^{(j)}) \in \mathbb{R}^J.$$

For $\mathbf{s} \in \mathbb{R}^J$, define $G : \mathbb{R}^J \rightarrow \mathbb{R}^J$ to be the sample mean of \mathbf{K}_t over $\{\nabla\phi_{\mathbf{s}}(X_t^{(j)})\}_{j=1}^J$,

$$G(\mathbf{s}) = \frac{1}{J} \sum_{j=1}^J \mathbf{K}_t(\nabla\phi_{\mathbf{s}}(X_t^{(j)})) = \frac{1}{J} \sum_{j=1}^J \mathbf{K}_t(X_t^{(j)} + \mathbf{s}^\top \nabla\mathbf{K}_t(X_t^{(j)})).$$

In order for sample-equivalence to be satisfied, we need to find \mathbf{s}^* such that $G(\mathbf{s}^*) = \mathbf{b}$.

Kuang and Tabak [31] demonstrate that if the Jacobian of G at $\mathbf{s} = \mathbf{0}$

$$\nabla G(\mathbf{s})|_{\mathbf{s}=\mathbf{0}} = \frac{1}{J} \sum_{i=1}^J \nabla\mathbf{K}_t(X_t^{(i)}) \nabla\mathbf{K}_t(X_t^{(i)})^\top \equiv M_t$$

is nonsingular (for which the necessary condition $J \leq dJ$ is automatically satisfied), G is a bijection from a neighborhood U about $\mathbf{s} = \mathbf{0}$ to a neighborhood V about $G(\mathbf{0}) = \mathbf{a}$. If $\mathbf{b} \in V$, then the potential $\phi_{\mathbf{s}}$ parameterized with $\mathbf{s}^* = G^{-1}(\mathbf{b})$ gives the *global minimum* of the sample-based OT problem (13) restricted to maps of the form (10). Furthermore, [31] shows that if the kernels are C^2 , then $\phi_{\mathbf{s}^*}$ is locally convex.

For sufficiently small Δt , the system $G(\mathbf{s}^*) = \mathbf{b}$ (12) will be close to linear. Thus, for the sake of computational efficiency we may approximate \mathbf{s}^* using a single Newton step, setting

$$\mathbf{s}^* \approx - \left(\frac{1}{J} \sum_{i=1}^J \nabla\mathbf{K}_t(X_t^{(i)}) \nabla\mathbf{K}_t(X_t^{(i)})^\top \right)^{-1} \sum_{k=1}^J \left(\frac{1}{J} - w_t^{(k)} \right) \mathbf{K}_t(X_t^{(k)}),$$

to arrive at the update

$$X_{t+\Delta t}^{(j)} = X_t^{(j)} - \left(\nabla_1 K(X_t^{(j)}, X_t^{(1)}) \quad \cdots \quad \nabla_1 K(X_t^{(j)}, X_t^{(J)}) \right) M_t^{-1} \sum_{k=1}^J \left(\frac{1}{J} - w_t^{(k)} \right) \begin{pmatrix} K(X_t^{(k)}, X_t^{(1)}) \\ \vdots \\ K(X_t^{(k)}, X_t^{(J)}) \end{pmatrix},$$

$$j = 1, \dots, J, \quad t \in [0, 1], \quad \{X_0^{(j)}\}_{j=1}^J \stackrel{\text{i.i.d.}}{\sim} \pi_0. \quad (14)$$

Although (14) is distinct from (7) in discrete time, in *continuous* time the two interacting particle systems are equivalent:

Theorem 2 *In the limit $\Delta t \rightarrow 0$, Equation (14) approaches Equation (7)*

$$\dot{X}_t^{(j)} = \left(\nabla_1 K(X_t^{(j)}, X_t^{(1)}) \quad \cdots \quad \nabla_1 K(X_t^{(j)}, X_t^{(J)}) \right) M_t^{-1} \cdot \frac{1}{J} \sum_{k=1}^J \left(\log \frac{\pi_1}{\pi_0}(X_t^{(k)}) - \log \frac{\pi_1}{\pi_0}(X_t^{(i)}) \right) \begin{pmatrix} K(X_t^{(k)}, X_t^{(1)}) \\ \vdots \\ K(X_t^{(k)}, X_t^{(J)}) \end{pmatrix},$$

with $t \in [0, 1]$ and $\{X_0^{(j)}\}_{j=1}^J \stackrel{\text{i.i.d.}}{\sim} \pi_0$. Thus, in the limit $J \rightarrow \infty$ and $\Delta t \rightarrow 0$, the IPS obtained via sample-driven optimal transport (14) approaches the mean-field model (6).

Proof: See Appendix A.2.

Owing to this equivalence in continuous time, we refer to the interacting particle system (14) as **KFRFlow-Importance (KFRFlow-I)**.

Theorem 2 highlights the fact that linearizing a Monge–Ampère equation for *static* optimal transport between π_t and $\pi_{t+\Delta t}$ results in a Poisson equation, and demonstrates that as $\Delta t \rightarrow 0$ this linearization yields the correct velocity field for the controlled *dynamic* minimum-energy transport problem of Section 3. Furthermore, it elucidates the connection between SMC approaches based on tempered self-normalized importance sampling and Fisher–Rao gradient flows.

5 Numerical examples

KFRFlow (7) can be discretized in time, for example, via the explicit Euler method

$$X_{t+\Delta t}^{(j)} = X_t^{(j)} + \left(\nabla_1 K(X_t^{(j)}, X_t^{(1)}) \quad \dots \quad \nabla_1 K(X_t^{(j)}, X_t^{(J)}) \right) M_t^{-1} \\ + \frac{\Delta t}{J} \sum_{k=1}^J \left(\log \frac{\pi_1}{\pi_0}(X_t^{(k)}) - \frac{1}{J} \sum_{i=1}^J \log \frac{\pi_1}{\pi_0}(X_t^{(i)}) \right) \begin{pmatrix} K(X_t^{(k)}, X_t^{(1)}) \\ \vdots \\ K(X_t^{(k)}, X_t^{(J)}) \end{pmatrix}, \quad j = 1, \dots, J \quad (15)$$

or any other standard ODE integration scheme, while KFRFlow-I (14) already has the form of a discrete-time iteration. In either case we start from $\{X_0^{(j)}\}_{j=1}^J \stackrel{\text{i.i.d.}}{\sim} \pi_0$ and simulate for unit time to obtain $\{X_1^{(j)}\}_{j=1}^J \sim \pi_{X_1} \approx \pi_1$. KFRFlow-I (14) and the Euler discretization of KFRFlow (15) are almost identical, and (14) can be recovered, up to multiplication by a constant close to one, from (15) using the approximation $\Delta t \log y = \log y^{\Delta t} \approx y^{\Delta t} - 1$ for $y \approx 1$. Our preliminary experiments do not indicate a clear pattern of when KFRFlow is preferable to KFRFlow-I or vice versa; hence we exercise them both here to demonstrate proof-of-concept.

We apply KFRFlow (7) and KFRFlow-I (14) to sample three two-dimensional densities demonstrating different behaviors along the evolution $\pi_t \propto \pi_0^t \pi_1^{1-t}$. In all three cases we take the reference π_0 to be standard Gaussian $\mathcal{N}(0, I_2)$ and π_1 to be a Bayesian posterior proportional to $\pi_0 \ell$ for a likelihood $\ell = \pi(y^* | \cdot)$ of the form

$$\ell(x) \propto \exp \left(-\frac{1}{\sigma_\epsilon^2} \|y^* - G(x)\|_2^2 \right),$$

i.e., $y^* \in \mathbb{R}$ is Gaussian with mean $G(x)$ and variance σ_ϵ^2 . Definitions of the three likelihoods and descriptions of the deformation behavior they entail can be found in Table 1.

$G(x)$	y^*	σ_ϵ^2	Behavior	Nickname
$\sqrt{x_1^2 + x_2^2}$	2	0.25^2	Concentration	Donut
$\sin(x_2) + \cos(x_1)$	-1	0.6^2	Bimodality	Butterfly
$\sin(x_1 x_2) + \cos(x_1 x_2)$	-1	0.5^2	Multimodality	Spaceships

Table 1: Likelihoods for the two-dimensional Bayesian example problems

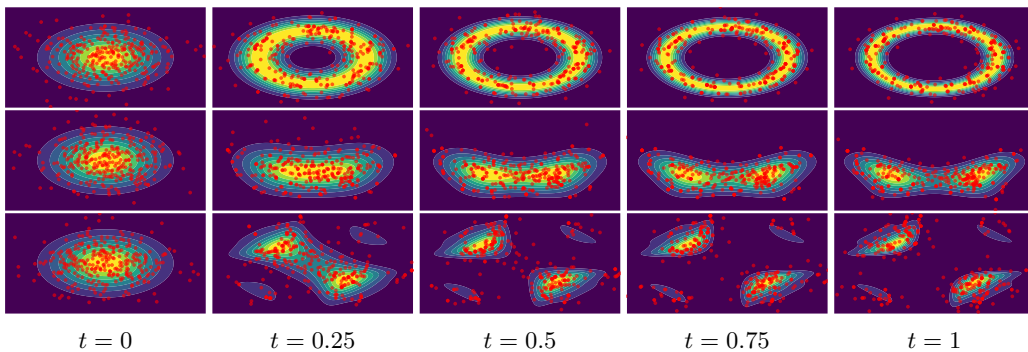


Figure 2: Samples at $t \in \{0, 0.25, 0.5, 0.75, 1\}$ generated by the IPS (7) for the donut (top), butterfly (middle), and spaceships (bottom) examples.

In all three examples we take the kernel $K(\cdot, \cdot)$ to be inverse multiquadric (IMQ)

$$K(x, x') = \left(1 + \frac{\|x - x'\|^2}{h^2} \right)^{-1/2} \quad (16)$$

with bandwidth $h > 0$ selected at each step of the iterations according to the median heuristic [35].

Figure 2 displays $J = 300$ samples obtained by running an explicit Euler discretization of KFRFlow (7) at times $t \in \{0.0, 0.25, 0.5, 0.75, 1.0\}$ with uniform timestep set to $\Delta t = 0.01$. The samples at $t = 1$ are qualitatively consistent with the target densities for each example, in particular even for the multimodal spaceships example wherein all four modes are sampled.

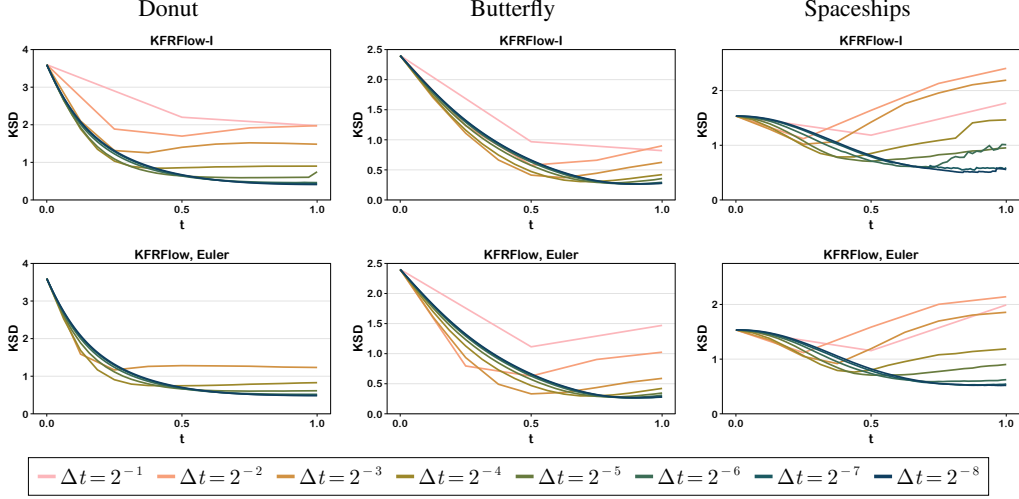


Figure 3: KSD as a function of time for KFRFlow-I (top) and an explicit Euler discretization of KFRFlow (bottom) for difference choices of Δt , averaged over 30 repeated trials, for the donut (left), butterfly (center), and spaceships (right) examples. In each example Δt must be below a certain threshold to ensure that KSD decreases monotonically throughout the iteration. KFRFlow-I seems to be more stable at large Δt than the Euler discretization of KFRFlow.

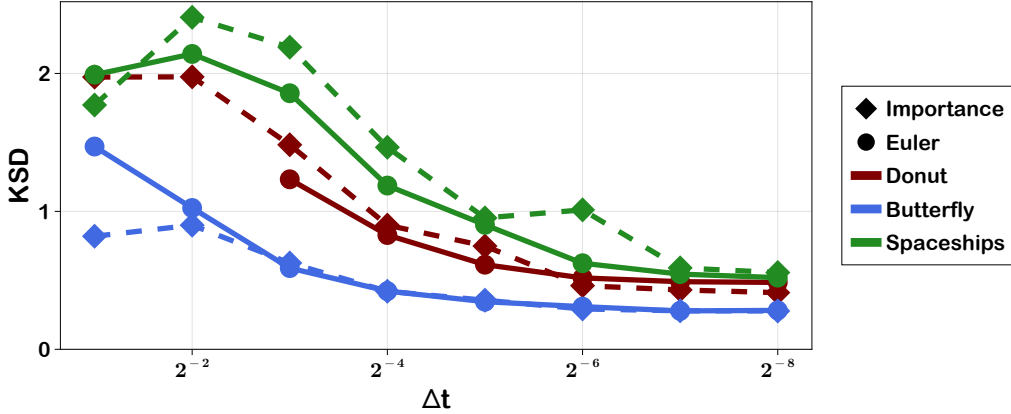


Figure 4: Average KSD as a function of time-step Δt between $J = 300$ samples computed with KFRFlow-I (dashed lines/diamonds) and an Euler discretization KFRFlow (solid lines/circles), where π_1 is the donut (maroon), butterfly (blue), or spaceships (green) example.

In Figures 3 and 4 we investigate the impact of step-size Δt and choice of interacting particle system – an explicit Euler discretization of KFRFlow (7) or KFRFlow-I (14) – on sample quality as measured by Kernel Stein Discrepancy (KSD) [24] using the IMQ kernel (16) with bandwidth $h = 1$. For each example we generate $J = 300$ approximate samples of π_1 via the iterations (14) and (15) for each $\Delta t \in \{2^{-1}, 2^{-2}, \dots, 2^{-8}\}$ and compute KSD between the samples and π_1 at each step of the iterations. The data plotted in Figures 3 and 4 are the result of averaging these KSD values over 30 repeated trials at each setting of Δt .

In Figure 3 we demonstrate the evolution of KSD as a function of t for various settings of Δt . For each example there seems to be a threshold Δt above which simulation of the interacting particle systems (14) and (15) will not result in a monotonic decrease of KSD with t . We see this behavior particularly in the donut and spaceships examples: in the donut example KSD increased by orders of magnitude relative to the starting KSD for the two largest Δt using the Euler discretization of KFRFlow, hence why those trajectories do not appear on the chart. In the spaceships example it is necessary to take $\Delta t \leq 2^{-4}$ to ensure that KSD does not increase relative to its starting value. We posit that the ODE (7) is stiffer in the spaceships and donut examples than in the butterfly example and that larger settings of Δt could be fruitfully used with higher-order ODE solvers.

In Figure 4 we plot the final-time KSD ($t = 1$) as a function of Δt for KFRFlow-I and the explicit Euler discretization of KFRFlow. The performances of the two interacting particle systems are generally comparable, and sample quality improves (KSD decreases) with decreasing Δt . As discussed previously, the Euler discretization of KFRFlow (15) is unstable in the donut example for the two largest Δt , hence why those datapoints are not visible in Figure 4. KFRFlow-I seems to have an advantage for large Δt , perhaps because it is explicitly designed for the purpose of obtaining incrementally accurate transport.

Across examples and choices of Δt we notice that the matrix M_t in the Euler iteration (15) may sometimes be poorly conditioned. We mitigate this problem by applying inflation, replacing M_t with $M_{t,\lambda} = M_t + \lambda I$ for some $\lambda > 0$. The Euler results for the donut, butterfly, and spaceships examples in Figure 4 are reflective of setting $\lambda = 0.1$, $\lambda = 10^{-8}$, and $\lambda = 10^{-11}$, respectively. Interestingly, KFRFlow-I (14) does not seem to suffer from the same level of instability as the Euler discretization of KFRFlow, and we thus do not inflate M_t in KFRFlow-I.

6 Discussion and future work

We have introduced a mean-field ODE model and corresponding Kernel Fisher–Rao Flow (KFRFlow) interacting particle systems which approximately transport samples from π_0 to π_1 in unit time. We obtain the mean-field ODE by solving an elliptic PDE arising from the Fisher–Rao gradient flow of the negative log likelihood under the ansatz that the solution lies in a reproducing kernel Hilbert space. The RKHS form of the mean-field ODE gives rise to tractable, gradient-free interacting particle systems for sampling. There are several lines of inquiry which would enhance our understanding of the mean-field model (6) and interacting particle systems KFRFlow (7) and KFRFlow-I (14), chief among them being quantifying approximation error and understanding sample complexity. It would also be interesting to determine whether the kernel approximation we have applied to the velocity field in our flow gives rise to some notion of a kernelized Fisher–Rao geometry for probability measures, in a similar vein to how SVGD can be viewed as arising from a gradient flow in a kernelized Wasserstein geometry [18].

Numerically we have seen that the quality of samples produced by KFRFlow and KFRFlow-I is good and generally improves with decreasing Δt . However, there are some settings of π_0 and π_1 which pose challenges for our algorithms, challenges which we suspect arise when the intersection of the effective supports of π_0 and π_1 is small. We are working to mitigate these challenges, develop better numerical implementations, and run detailed performance comparisons of KFRFlow and KFRFlow-I to similar algorithms such as EKI [27] and SVGD [35].

Finally, our approach has connections to other sampling algorithms which employ the geometric mixture $\pi_t \propto \pi_0^{1-t} \pi_1^t$ or require solutions of Poisson’s equation, including the data assimilation frameworks of [42, 13], ensemble Kalman inversion [27], the feedback particle filter [59, 53], and tempered SMC algorithms [4, 30, 10, 25]. We seek to further understand these connections and use them to design new and better sampling algorithms in the vein of what we have introduced here.

Acknowledgments and Disclosure of Funding

AM and YM were supported by the Office of Naval Research, SIMDA (Sea Ice Modeling and Data Assimilation) MURI, award number N00014-20-1-2595 (Dr. Reza Malek-Madani and Dr. Scott Harper). AM was additionally supported by the NSF Graduate Research Fellowship under Grant No. 1745302.

A Supplementary Material

A.1 Proof of Theorem 1

Notice that as $J \rightarrow \infty$ and for any $x \in \mathbb{R}^d$ the sum

$$\frac{1}{J} \sum_{k=1}^J \left(\log \frac{\pi_1}{\pi_0}(X_t^{(k)}) - \sum_{i=1}^J \log \frac{\pi_1}{\pi_0}(X_t^{(i)}) \right) K(X_t^{(k)}, x)$$

approaches the kernelization of $\log \frac{\pi_1}{\pi_0}(\cdot) - \mathbb{E}_{\rho_t}[\log \frac{\pi_1}{\pi_0}]$ with respect to $\rho_t = \text{Law}(X_t)$,

$$K_{\rho_t} \left(\log \frac{\pi_1}{\pi_0}(\cdot) - \mathbb{E}_{\rho_t}[\log \frac{\pi_1}{\pi_0}] \right) (x) \equiv \int_{\mathbb{R}^d} (\log \frac{\pi_1}{\pi_0}(z) - \mathbb{E}_{\rho_t}[\log \frac{\pi_1}{\pi_0}]) K(z, x) d\rho_t(z).$$

Hence, as $J \rightarrow \infty$ the vector

$$\frac{1}{J} \sum_{k=1}^J \left(\log \frac{\pi_1}{\pi_0}(X_t^{(k)}) - \sum_{i=1}^J \log \frac{\pi_1}{\pi_0}(X_t^{(i)}) \right) \begin{pmatrix} K(X_t^{(k)}, X_t^{(1)}) \\ \dots \\ K(X_t^{(k)}, X_t^{(J)}) \end{pmatrix}$$

can be replaced by the function $x \mapsto K_{\rho_t} \left(\log \frac{\pi_1}{\pi_0}(\cdot) - \mathbb{E}_{\rho_t}[\log \frac{\pi_1}{\pi_0}] \right) (x)$.

Similarly, as $J \rightarrow \infty$, M_t can be viewed as a kernel $M_t : \mathbb{R}^d \times \mathbb{R}^d \rightarrow \mathbb{R}$

$$M_t(z, z') = \mathbb{E}_{X_t \sim \rho_t} \langle \nabla_1 K(X_t, z), \nabla_1 K(X_t, z') \rangle,$$

which can be applied to functions on \mathbb{R}^d as a convolution-type operator with respect to ρ_t ,

$$M_{\rho_t} f(x) = \int_{\mathbb{R}^d} f(z) M_t(x, z) d\rho_t(z) = \iint_{\mathbb{R}^d \times \mathbb{R}^d} f(z) \langle \nabla_1 K(y, x), \nabla_1 K(y, z) \rangle d\rho_t(y) d\rho_t(z).$$

Denoting by $M_{\rho_t}^{-1}$ the inverse operator to M_{ρ_t} , the mean-field limit of (7) can be written

$$\begin{aligned} \dot{X}_t^{(j)} &\stackrel{J \rightarrow \infty}{\rightarrow} \int_{\mathbb{R}^d} \nabla_1 K(X_t^{(j)}, x) M_{\rho_t}^{-1} K_{\rho_t} \left(\log \frac{\pi_1}{\pi_0}(\cdot) - \mathbb{E}_{\rho_t} \left[\log \frac{\pi_1}{\pi_0} \right] \right) (x) d\rho_t(x) \\ &= \mathbb{E}_{X \sim \rho_t} \left[\nabla_1 K(X_t^{(j)}, X) M_{\rho_t}^{-1} K_{\rho_t} \left(\log \frac{\pi_1}{\pi_0}(\cdot) - \mathbb{E}_{\rho_t} \left[\log \frac{\pi_1}{\pi_0} \right] \right) (X) \right]. \end{aligned}$$

A.2 Proof of Theorem 2

Notice that time only enters the update equation (14) through the importance weights $w_t^{(k)}$. To obtain the continuous time limiting ODE we rearrange, divide by Δt on both sides, and take $\Delta t \rightarrow 0$,

$$\lim_{\Delta t \rightarrow 0} \frac{X_{t+\Delta t}^{(j)} - X_t^{(j)}}{\Delta t} = \lim_{\Delta t \rightarrow 0} - \left(\nabla_1 K(X_t^{(j)}, X_t^{(1)}) \quad \dots \quad \nabla_1 K(X_t^{(j)}, X_t^{(J)}) \right) M_t^{-1} \sum_{k=1}^J \frac{\frac{1}{J} - w_t^{(k)}}{\Delta t} \begin{pmatrix} K(X_t^{(k)}, X_t^{(1)}) \\ \vdots \\ K(X_t^{(k)}, X_t^{(J)}) \end{pmatrix}.$$

Examining the terms above involving Δt , we see that for $k \in \{1, \dots, J\}$ we have

$$\begin{aligned} \lim_{\Delta t \rightarrow 0} \frac{\frac{1}{J} - w_t^{(k)}}{\Delta t} &= - \lim_{\Delta t \rightarrow 0} \frac{\frac{(\frac{\pi_1}{\pi_0}(X_t^{(k)}))^{\Delta t}}{\sum_{i=1}^J (\frac{\pi_1}{\pi_0}(X_t^{(i)}))^{\Delta t}} - \frac{1}{J}}{\Delta t} = - \lim_{\Delta t \rightarrow 0} \frac{\frac{(\frac{\pi_1}{\pi_0}(X_t^{(k)}))^{\Delta t}}{\sum_{i=1}^J (\frac{\pi_1}{\pi_0}(X_t^{(i)}))^{\Delta t}} - \frac{(\frac{\pi_1}{\pi_0}(X_t^{(k)}))^0}{\sum_{i=1}^J (\frac{\pi_1}{\pi_0}(X_t^{(i)}))^0}}{\Delta t} \\ &= - \frac{d}{d\Delta t} \frac{(\frac{\pi_1}{\pi_0}(X_t^{(k)}))^{\Delta t}}{\sum_{i=1}^J (\frac{\pi_1}{\pi_0}(X_t^{(i)}))^{\Delta t}} \Big|_{\Delta t=0} \\ &= - \frac{(\frac{\pi_1}{\pi_0}(X_t^{(k)}))^{\Delta t} \log \frac{\pi_1}{\pi_0}(X_t^{(k)}) \sum_{i=1}^J (\frac{\pi_1}{\pi_0}(X_t^{(i)}))^{\Delta t} - (\frac{\pi_1}{\pi_0}(X_t^{(k)}))^{\Delta t} \sum_{i=1}^J (\frac{\pi_1}{\pi_0}(X_t^{(i)}))^{\Delta t} \log \frac{\pi_1}{\pi_0}(X_t^{(i)})}{\left(\sum_{i=1}^J (\frac{\pi_1}{\pi_0}(X_t^{(i)}))^{\Delta t} \right)^2}} \Big|_{\Delta t=0} \\ &= - \frac{J \log \frac{\pi_1}{\pi_0}(X_t^{(k)}) - \sum_{i=1}^J \log \frac{\pi_1}{\pi_0}(X_t^{(i)})}{J^2} = - \frac{1}{J} \left(\log \frac{\pi_1}{\pi_0}(X_t^{(k)}) - \frac{1}{J} \sum_{i=1}^J \log \frac{\pi_1}{\pi_0}(X_t^{(i)}) \right). \end{aligned}$$

Hence, the ODE arising from the limit of (14) as $\Delta t \rightarrow 0$ is (7)

$$\begin{aligned} \dot{X}_t^{(j)} &= \left(\nabla_1 K(X_t^{(j)}, X_t^{(1)}) \quad \dots \quad \nabla_1 K(X_t^{(j)}, X_t^{(J)}) \right) M_t^{-1} \\ &\quad \frac{1}{J} \sum_{k=1}^J \left(\log \frac{\pi_1}{\pi_0}(X_t^{(k)}) - \frac{1}{J} \sum_{i=1}^J \log \frac{\pi_1}{\pi_0}(X_t^{(i)}) \right) \begin{pmatrix} K(X_t^{(k)}, X_t^{(1)}) \\ \vdots \\ K(X_t^{(k)}, X_t^{(J)}) \end{pmatrix}, \end{aligned}$$

with initial condition $\{X_0^{(j)}\}_{j=1}^J \stackrel{\text{i.i.d.}}{\sim} \pi_0$. Thus, by Theorem 1, the mean-field, continuous-time limit of (14) is (6).

References

- [1] M. S. Albergo, N. M. Boffi, and E. Vanden-Eijnden, “Stochastic Interpolants: A Unifying Framework for Flows and Diffusions,” no. arXiv:2303.08797, Mar. 2023.
- [2] R. Baptista, B. Hosseini, N. B. Kovachki, and Y. Marzouk, “Conditional Sampling with Monotone GANs: From Generative Models to Likelihood-Free Inference,” no. arXiv:2006.06755, Jun. 2023.
- [3] R. Baptista, Y. Marzouk, and O. Zahm, “On the representation and learning of monotone triangular transport maps,” *Foundations of Computational Mathematics*, vol. in press, 2023, arXiv:2009.10303.
- [4] R. Breckelmanns, V. Masrani, T. Bui, F. Wood, A. Galstyan, G. V. Steeg, and F. Nielsen, “Annealed Importance Sampling with q-Paths,” no. arXiv:2012.07823, Dec. 2020.
- [5] Y. Brenier, “Polar factorization and monotone rearrangement of vector-valued functions,” *Communications on pure and applied mathematics*, vol. 44, no. 4, pp. 375–417, 1991.
- [6] M. C. Brennan, D. Bigoni, O. Zahm, A. Spantini, and Y. Marzouk, “Greedy inference with structure-exploiting lazy maps,” *Advances in Neural Information Processing Systems*, vol. 33, pp. 8330–8342, 2020.
- [7] C. Bunne, A. Krause, and M. Cuturi, “Supervised training of conditional Monge maps,” *Advances in Neural Information Processing Systems*, vol. 35, pp. 6859–6872, 2022.
- [8] P. Chen, K. Wu, J. Chen, T. O’Leary-Roseberry, and O. Ghattas, “Projected Stein variational Newton: A fast and scalable Bayesian inference method in high dimensions,” *Advances in Neural Information Processing Systems*, vol. 32, 2019.
- [9] Y. Chen, D. Z. Huang, J. Huang, S. Reich, and A. M. Stuart, “Gradient Flows for Sampling: Mean-Field Models, Gaussian Approximations and Affine Invariance,” Jul. 2023.
- [10] N. Chopin, F. R. Crucinio, and A. Korba, “A connection between tempering and entropic mirror descent,” *arXiv preprint arXiv:2310.11914*, 2023.
- [11] B. Dai and U. Seljak, “Sliced Iterative Normalizing Flows,” in *Proceedings of the 38th International Conference on Machine Learning*. PMLR, Jul. 2021, pp. 2352–2364.
- [12] F. Daum and J. Huang, “Particle flow for nonlinear filters,” in *2011 IEEE International Conference on Acoustics, Speech and Signal Processing (ICASSP)*. IEEE, 2011, pp. 5920–5923.
- [13] —, “Particle flow for nonlinear filters, Bayesian decisions and transport,” in *Proceedings of the 16th International Conference on Information Fusion*. IEEE, 2013, pp. 1072–1079.
- [14] V. De Bortoli, J. Thornton, J. Heng, and A. Doucet, “Diffusion Schrödinger bridge with applications to score-based generative modeling,” in *Advances in Neural Information Processing Systems*, vol. 34. Curran Associates, Inc., 2021, pp. 17 695–17 709. [Online]. Available: <https://proceedings.neurips.cc/paper/2021/hash/940392f5f32a7ade1cc201767cf83e31-Abstract.html>
- [15] P. Del Moral, A. Doucet, and A. Jasra, “Sequential Monte Carlo samplers,” *Journal of the Royal Statistical Society Series B: Statistical Methodology*, vol. 68, no. 3, pp. 411–436, 2006.
- [16] B. M. Dia, “A Continuation Method in Bayesian Inference,” *SIAM/ASA Journal on Uncertainty Quantification*, pp. 646–681, Jun. 2023.
- [17] Z. Ding and Q. Li, “Ensemble Kalman inversion: Mean-field limit and convergence analysis,” *Statistics and Computing*, vol. 31, no. 1, p. 9, Jan. 2021.
- [18] A. Duncan, N. Nüsken, and L. Szpruch, “On the geometry of Stein variational gradient descent,” *Journal of Machine Learning Research*, vol. 24, no. 56, pp. 1–39, 2023.
- [19] D. J. Earl and M. W. Deem, “Parallel tempering: Theory, applications, and new perspectives,” *Physical Chemistry Chemical Physics*, vol. 7, no. 23, pp. 3910–3916, 2005.

- [20] L. C. Evans, “Partial differential equations and Monge-Kantorovich mass transfer,” *Current developments in mathematics*, vol. 1997, no. 1, pp. 65–126, 1997.
- [21] A. Garbuno-Inigo, F. Hoffmann, W. Li, and A. M. Stuart, “Interacting Langevin Diffusions: Gradient Structure and Ensemble Kalman Sampler,” *SIAM Journal on Applied Dynamical Systems*, vol. 19, no. 1, pp. 412–441, Jan. 2020.
- [22] A. Garbuno-Inigo, N. Nüsken, and S. Reich, “Affine Invariant Interacting Langevin Dynamics for Bayesian Inference,” *SIAM Journal on Applied Dynamical Systems*, Jul. 2020.
- [23] C. J. Geyer, “Markov chain Monte Carlo maximum likelihood,” 1991.
- [24] J. Gorham and L. Mackey, “Measuring Sample Quality with Kernels,” Oct. 2020.
- [25] S. Goshtasbpour, V. Cohen, and F. Perez-Cruz, “Adaptive annealed importance sampling with constant rate progress,” in *International Conference on Machine Learning*. PMLR, 2023, pp. 11 642–11 658.
- [26] J. Heng, V. De Bortoli, and A. Doucet, “Diffusion Schrödinger bridges for Bayesian computation,” no. arXiv:2308.14106, Aug. 2023.
- [27] M. A. Iglesias, K. J. H. Law, and A. M. Stuart, “Ensemble Kalman methods for inverse problems,” *Inverse Problems*, vol. 29, no. 4, p. 045001, Apr. 2013.
- [28] M. Katzfuss and F. Schäfer, “Scalable Bayesian Transport Maps for High-Dimensional Non-Gaussian Spatial Fields,” *Journal of the American Statistical Association*, vol. 0, no. 0, pp. 1–15, 2023.
- [29] I. Kobyzev, S. J. Prince, and M. A. Brubaker, “Normalizing flows: An introduction and review of current methods,” *IEEE transactions on pattern analysis and machine intelligence*, vol. 43, no. 11, pp. 3964–3979, 2020.
- [30] A. Korba and F. Portier, “Adaptive importance sampling meets mirror descent: a bias-variance tradeoff,” in *International Conference on Artificial Intelligence and Statistics*. PMLR, 2022, pp. 11 503–11 527.
- [31] M. Kuang and E. G. Tabak, “Sample-Based Optimal Transport and Barycenter Problems,” *Communications on Pure and Applied Mathematics*, vol. 72, no. 8, pp. 1581–1630, 2019.
- [32] H. R. Künsch, “Recursive Monte Carlo filters: Algorithms and theoretical analysis,” *The Annals of Statistics*, vol. 33, no. 5, pp. 1983 – 2021, 2005. [Online]. Available: <https://doi.org/10.1214/009053605000000426>
- [33] R. S. Laugesen, P. G. Mehta, S. P. Meyn, and M. Raginsky, “Poisson’s equation in nonlinear filtering,” *SIAM Journal on Control and Optimization*, vol. 53, no. 1, pp. 501–525, 2015.
- [34] Y. Lipman, R. T. Q. Chen, H. Ben-Hamu, M. Nickel, and M. Le, “Flow matching for generative modeling,” no. arXiv:2210.02747, 2023. [Online]. Available: <http://arxiv.org/abs/2210.02747>
- [35] Q. Liu and D. Wang, “Stein Variational Gradient Descent: A General Purpose Bayesian Inference Algorithm,” in *Advances in Neural Information Processing Systems*, vol. 29. Curran Associates, Inc., 2016.
- [36] X. Liu, C. Gong, and Q. Liu, “Flow straight and fast: Learning to generate and transfer data with rectified flow,” no. arXiv:2209.03003, 2022. [Online]. Available: <http://arxiv.org/abs/2209.03003>
- [37] Y. Marzouk, T. Moselhy, M. Parno, and A. Spantini, “Sampling via measure transport: An introduction,” *Handbook of uncertainty quantification*, vol. 1, p. 2, 2016.
- [38] R. M. Neal, “Annealed importance sampling,” *Statistics and computing*, vol. 11, pp. 125–139, 2001.
- [39] A. B. Owen, *Monte Carlo theory, methods and examples*. <https://artowen.su.domains/mc/>, 2013.

- [40] G. Papamakarios, E. Nalisnick, D. J. Rezende, S. Mohamed, and B. Lakshminarayanan, “Normalizing flows for probabilistic modeling and inference,” *The Journal of Machine Learning Research*, vol. 22, no. 1, pp. 2617–2680, 2021.
- [41] M. Ramgraber, R. Baptista, D. McLaughlin, and Y. Marzouk, “Ensemble transport smoothing—part 2: nonlinear updates,” *arXiv preprint arXiv:2210.17435*, 2022.
- [42] S. Reich, “A dynamical systems framework for intermittent data assimilation,” *BIT Numerical Mathematics*, vol. 51, no. 1, pp. 235–249, Mar. 2011.
- [43] —, “A Nonparametric Ensemble Transform Method for Bayesian Inference,” *SIAM Journal on Scientific Computing*, vol. 35, no. 4, pp. A2013–A2024, Jan. 2013. [Online]. Available: <http://epubs.siam.org/doi/10.1137/130907367>
- [44] S. Reich and S. Weissmann, “Fokker–Planck Particle Systems for Bayesian Inference: Computational Approaches,” *SIAM/ASA Journal on Uncertainty Quantification*, vol. 9, no. 2, pp. 446–482, Jan. 2021.
- [45] D. Rezende and S. Mohamed, “Variational inference with normalizing flows,” in *International conference on machine learning*. PMLR, 2015, pp. 1530–1538.
- [46] C. Snyder, T. Bengtsson, P. Bickel, and J. Anderson, “Obstacles to high-dimensional particle filtering,” *Monthly Weather Review*, vol. 136, no. 12, pp. 4629–4640, 2008.
- [47] Y. Song, J. Sohl-Dickstein, D. P. Kingma, A. Kumar, S. Ermon, and B. Poole, “Score-based generative modeling through stochastic differential equations,” in *International conference on learning representations*, 2021.
- [48] A. Spantini, D. Bigoni, and Y. Marzouk, “Inference via low-dimensional couplings,” *The Journal of Machine Learning Research*, vol. 19, no. 1, pp. 2639–2709, 2018.
- [49] A. Spantini, R. Baptista, and Y. Marzouk, “Coupling Techniques for Nonlinear Ensemble Filtering,” *SIAM Review*, vol. 64, no. 4, pp. 921–953, Nov. 2022.
- [50] I. Steinwart and A. Christmann, *Kernels and Reproducing Kernel Hilbert Spaces*. New York, NY: Springer New York, 2008, pp. 110–163. [Online]. Available: https://doi.org/10.1007/978-0-387-77242-4_4
- [51] S. Syed, V. Romaniello, T. Campbell, and A. Bouchard-Côté, “Parallel tempering on optimized paths,” in *International Conference on Machine Learning*. PMLR, 2021, pp. 10 033–10 042.
- [52] A. Taghvaei and B. Hosseini, “An Optimal Transport Formulation of Bayes’ Law for Nonlinear Filtering Algorithms,” in *2022 IEEE 61st Conference on Decision and Control (CDC)*, Dec. 2022, pp. 6608–6613.
- [53] A. Taghvaei and P. G. Mehta, “A survey of feedback particle filter and related controlled interacting particle systems (CIPS),” *Annual Reviews in Control*, vol. 55, pp. 356–378, Jan. 2023.
- [54] G. Trigila and E. G. Tabak, “Data-Driven Optimal Transport,” *Communications on Pure and Applied Mathematics*, vol. 69, no. 4, pp. 613–648, 2016.
- [55] N. G. Trillos, B. Hosseini, and D. Sanz-Alonso, “From Optimization to Sampling Through Gradient Flows,” Feb. 2023.
- [56] F. Vargas, W. Grathwohl, and A. Doucet, “Denoising diffusion samplers,” *arXiv preprint arXiv:2302.13834*, 2023.
- [57] C. Villani, *Topics in Optimal Transportation*. American Mathematical Soc., Aug. 2021.
- [58] C. Xu, X. Cheng, and Y. Xie, “Optimal transport flow and infinitesimal density ratio estimation,” no. arXiv:2305.11857. [Online]. Available: <http://arxiv.org/abs/2305.11857>
- [59] T. Yang, P. G. Mehta, and S. P. Meyn, “Feedback Particle Filter,” *IEEE Transactions on Automatic Control*, vol. 58, no. 10, pp. 2465–2480, Oct. 2013.